
CHAPTER 3

From Surface to Image

3.1. Introduction

Given a light source, a surface, and an observer, a reflectance model describes the intensity and spectral composition of the reflected light reaching the observer. The intensity of the reflected light is determined by the intensity and size of the light source and by the reflecting ability and surface properties of the surface. In this chapter, we will discuss the modelling techniques from 3D surface to 2D image.

First all, we introduce surface roughness models, including height distribution model and slope distribution model, and then the illumination geometry used in this thesis is illustrated. Secondly, various reflection and illumination modelling is under the review. Therefore a simple Lambertian illumination model is presented to describe diffuse reflection. Thirdly, We present the Kube-Pentland's surface model, a linear Lambertian model used in this thesis. A deep investigation about this model is given, with regard to its frequency domain responses, directional filter, effect of non-linear and shadowing. Fourthly, four models of rough synthetic surfaces are given for the purpose of simulation process. Finally, we demonstrate that surface rotation classification is not equivalent to image rotation classification.

3.1.1. Surface Roughness

The manner in which light is reflected by a surface is dependent on the shape characteristics of the surface. In order to analyse the reflection of incident light, we must know the shape of the reflecting surface. In another words, we need a mathematical model of the surface. There are two ways to describe the model of surface and its roughness: the height distribution model and the slope distribution model [Nayar91]. A brief discussion of existing surface roughness models is given below, in order to identify significant limitations in currently applied methods.

- ***Height distribution model***

In height distribution model, the height coordinate of the surface may be expressed as a random function and then the shape of the surface is determined by the probability distribution of the height coordinates. The usual general measures of surface roughness are the standard deviation of the surface heights σ_s (root-mean-square roughness) and average roughness R_{cla} (Centre Line Average CLA), which can be obtained as follows:

$$\sigma_s = \sqrt{\frac{1}{n} \sum_{x=1}^n [s(x) - \overline{s(x)}]^2} \quad (3.1)$$

$$R_{cla} = \frac{1}{n} \sum_{x=1}^n |s(x)| \quad (3.2)$$

where $s(x)$ presents the height of a surface at a point x along the profile, $\overline{s(x)}$ is the expectation of $s(x)$ and n is the number of pixels. Hence, they provide measures of the average localised surface deviation about a nominal path. The shape or form of the textural surface cannot be implied from these measures. Indeed textures with differing physical characteristics may result in similar values [Smith99a]. We also have to note that the surface roughness cannot be defined by one of these parameters, either σ_s or R_{cla} , since two surfaces with the same height distribution function may not resemble each other in many cases [Nayar91]. Hence using such a model, it is difficult to derive a reflectance model for arbitrary source and viewer directions.

- ***Slope distribution model***

The slope distribution model is commonly utilised in the analysis of surface reflection as the scattering of light rays has been shown to be dependent on the local slope of the surface and not the local height of the surface. The slope model is therefore more suitable for investigation of the problem of surface reflection. It is useful to think of a surface as a collection of planar micro-facets, as illustrated in *Figure 3. 1*.

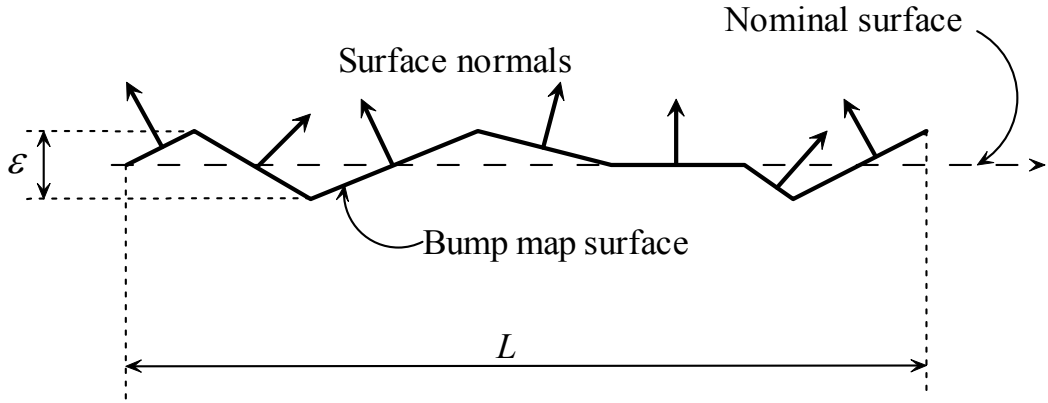


Figure 3. 1 A surface as a collection of planar micro-facets

If a surface is mathematically smooth and each facet area ε is small compared to the area L of the surface patch ($L \gg \varepsilon$), we may use two slope parameters, p_{rms} and q_{rms} , as a measure of roughness. They correspond to the standard deviation of the surface partial derivatives p and q .

$$p_{rms} = \sqrt{\frac{1}{n} \sum_{x=1}^n \left(\frac{\partial s(x, y)}{\partial x} - \overline{\frac{\partial s(x, y)}{\partial x}} \right)^2} \quad (3. 3)$$

$$q_{rms} = \sqrt{\frac{1}{n} \sum_{x=1}^n \left(\frac{\partial s(x, y)}{\partial y} - \overline{\frac{\partial s(x, y)}{\partial y}} \right)^2} \quad (3. 4)$$

where $\frac{\partial s(x, y)}{\partial x}$ and $\frac{\partial s(x, y)}{\partial y}$ are surface partial derivatives measured along the x and y axes respectively. Hence p_{rms} and q_{rms} can be used to describe surfaces with both isotropic and directional roughness.

3.1.2. Illumination Geometry

Before we consider the reflectance model which defines the relationship between a surface and the corresponding image intensities, we first give the definition of illumination angles related to the light source in *Figure 3. 2*. These definitions are used throughout this thesis. The imaging geometry assumptions are as follows:

- *the test surface* is mounted in the x - y plane and is perpendicular to the camera axis (the z -axis).
- the test surface is illuminated by *a point source* located at infinity, i.e. the incident vector field is uniform in magnitude and direction over the test area.
- *the tilt angle* τ of illumination is the angle that the projection of the illuminant vector incident onto the test surface plane makes with an axis in that plane.
- *the slant angle* σ is the angle that the illuminant vector makes with a normal to the test surface plane.
- *surface rotation* is measured in the x - y plane.
- *orthographic camera* model assumed.

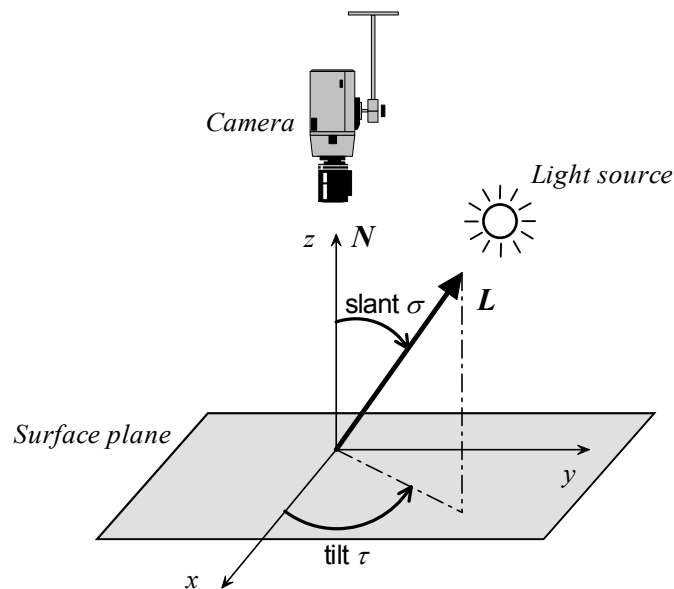


Figure 3. 2 Illumination geometry: the definitions of the tilt angle τ and the slant angle σ .

3.1.3. Diffuse and Specular

Reflection from smooth surfaces such as mirrors or a still body of water results in a type of reflection known *specular reflection*. Reflection from rough surfaces such as clothing, paper and an asphalt roadway produces a type of reflection known as *diffuse reflection*. In practice the reflection process may well be a combination of both diffuse and specular components. An example of this is a *spread reflection*, which has a dominant directional component that is partially diffused by surface irregularities. Whether the surface is microscopically rough or smooth has a tremendous impact upon the subsequent reflection of a beam of light. *Figure 3. 3* depicts a beam of light incident upon a surface and the resultant reflection for different types of surfaces. An example of diffuse and specular reflectance for a sphere is shown in *Figure 3. 4*.

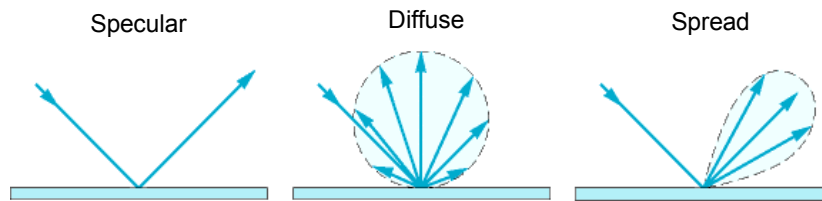


Figure 3. 3 Specular, diffuse and spread reflection from a surface.

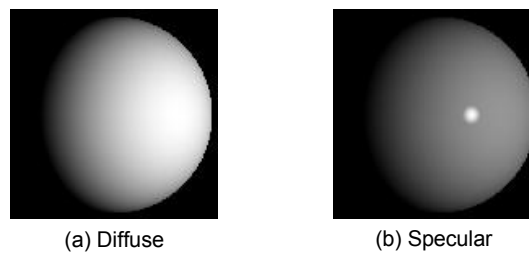


Figure 3. 4 An example of diffuse and specular reflectance.

Several models for the specular component have been proposed. Phong [Phong75] models a reflection lobe which was spread out around the specular direction by using a cosine function raised to a power. Blinn [Blinn77] proposed a model which accounts for off-specular peaks that occur when the incident light is at a grazing

angle. These models are relatively simple with regard to calculation and give reasonably realistic results.

In this thesis, we have to analyse both synthetic and real images, but only the diffuse reflection is taken into account in general. The specular reflection is simply disregarded as noise in most cases except for the method proposed in *Chapter 9*, where a method based on photometric stereo is developed which is similar to the approach by Coleman and Jain [Coleman82].

3.2. Reflection and Illumination modelling

The purpose of reflection models in computer vision is to enable the rendering of a 3D surface in 2D space, such that reality is mimicked to a reasonable level. An image of the surface results from light source reflected from the surface in the direction of the sensor. The intensity at any given point in the image is closely related to the reflectance properties of the corresponding point on the surface. Therefore the prediction or the interpretation of image intensities requires a sound understanding of the various mechanisms involved in the reflection process.

3.2.1. Review of Related Work

Various reflectance models have been developed in the field of computer vision. In general they can be classified into two categories: *the physical models and the geometrical models* in [Nayar91]. The physicals model use electromagnetic wave theory to analyse the reflection of incident light. This is more general than the models based on geometrical optics in that it can describe reflection from smooth to rough surfaces. However, physical models are often inappropriate for use in machine vision as they have functional forms which are difficult to manipulate. On the other hand, geometrical models are derived by analysing the surface and illumination geometry and have simpler functional forms.

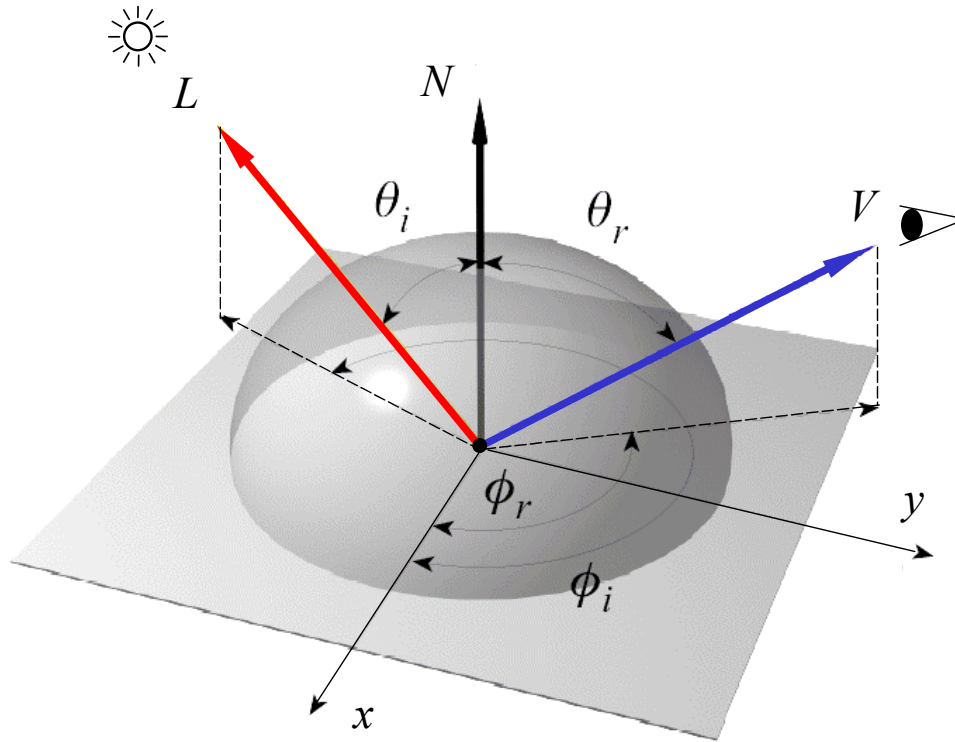


Figure 3. 5 The geometry of light reflection.

The geometry of light reflection at a surface is illustrated in *Figure 3. 5*. Reflection models are generally presented in terms of a *Bidirectional Reflectance Distribution Function (BRDF)*. The BRDF is a general model that relates the energy arriving at a surface from the direction of illumination, to the reflected intensity in the direction of the viewer:

$$BRDF(\lambda, \theta_i, \phi_i, \theta_r, \phi_r) \quad (3.5)$$

Where λ is the wavelength of the incident light, (θ_i, ϕ_i) is the direction of the incoming light and (θ_r, ϕ_r) is the direction of the reflected light shown in *Figure 3. 5*. The BRDF can be divided into three components: (a) *specular* component, (b) *directional diffuse* component and (c) *uniform diffuse* component demonstrated in *Figure 3. 6*.

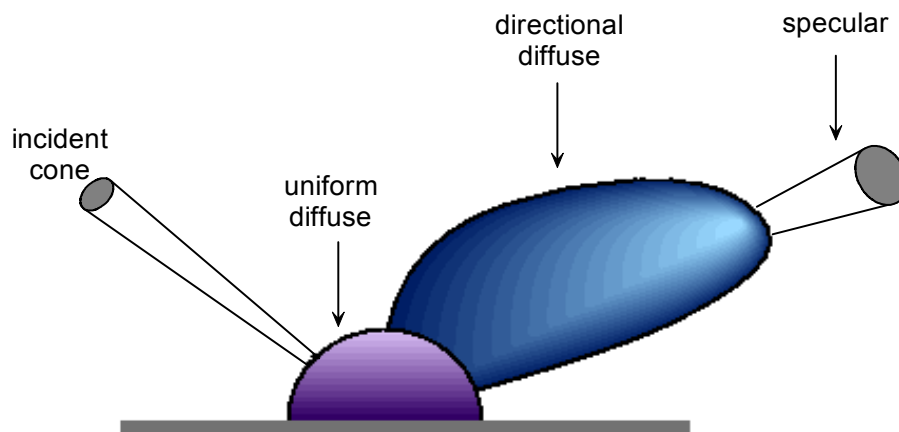


Figure 3. 6 Three components of BRDF: (1). uniform diffuse component; (2). directional diffuse component and (3). specular component.

Over the past twenty years, a variety of BRDF models of increasing sophistication have been proposed. He [He91] proposed a general light reflection model that assumes Gaussian, isotropic rough surface. The model is based on wave optics and accounts for diffraction and scattering effects. The model provides closed-form analytical expressions for the specular, directional diffuse and uniform diffuse components of the BRDF. One paper that does present a method for acquiring BRDFs is [Ward92]. Ward built an imaging reflectometer that uses the two degrees of freedom inherent in a camera imaging system to measure BRDFs and presented an “elliptical Gaussian” model that is capable of modelling certain kinds of anisotropy.

The Lambertian BRDF has enjoyed widespread use for modelling smooth matte surfaces. The Torrance-Sparrow model [Torrance67] for describing surface reflection from rough surfaces has been used extensively in computer vision and graphics. They have appended the Lambertian model to their reflectance model to account for the internal scattering mechanism. The surface is modelled as a collection of planar micro facets and the facet slopes are assumed to be normally distributed. Oren and Nayar [Oren95] derived a reflectance model for matte surfaces which includes local occlusions, shadowing and interreflections. Work by Wolff [Wolff96] developed a simple modification of Lambert’s law which accurately accounts for all illumination and viewing directions. Koenderink and van Doorn [Koenderink96] have measured the BRDFs for a variety of surfaces. Their measurements indicate they are fairly well

behaved and can be represented using a relatively small (50 or less) number of basis BRDFs.

The most commonly used model in computer vision is the Phong reflection model [Phong75], which is a linear combination of specular and diffuse reflection. The specular component is a lobe which spreads out around the specular direction and is modelled by using a cosine function raised to a power. Phong's model is usually given in terms of unit vectors associated with the geometry of the point under consideration:

$$I(n, \Phi) = I_a k_a + I_i k_d (\mathbf{L} \cdot \mathbf{N}) + I_i k_s (\mathbf{R} \cdot \mathbf{V})^n \quad (3.6)$$

where, I_a is the constant intensity of the ambient light;

k_a is the coefficient of ambient reflection of the surface;

I_i is the intensity of the incident light;

k_d is the coefficient of diffuse reflection for the material;

k_s is the coefficient of specular reflection;

Φ is the angle between the mirror vector \mathbf{R} and the viewing vector \mathbf{V} highlight shown in *Figure 3.7*, and

n is an index that controls the tightness of the specular lobe.

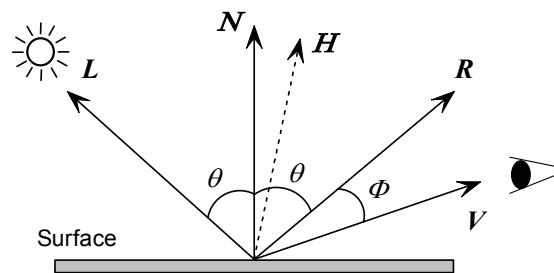


Figure 3.7 Vectors used in the Phong reflection model.

In Phong's model, the light sources are usually considered as point sources situated infinitely far away. Hence the angle θ between the incident light and the normal to a planar surface is constant over the surface. The viewer is assumed to be positioned at infinity and hence the angle Φ is constant over a planar surface as well. The diffuse and specular terms are modelled as local components only. Shadows are not

considered. The colour of the specular term is assumed to be that of the light source. Empirical results are used to model the distribution of the specular term around the reflection vector. It is also important to note that, unlike Lambert's law, this model has no physical interpretation; it follows nature in an empirical way only.

Estimating the specular component involves the computation of the reflected vector \mathbf{R} . This is somewhat computationally expensive and hence this is often replaced by the computation of \mathbf{H} , a vector half-way between \mathbf{L} and \mathbf{V} . This is often called Blinn's method [Blinn77]. Therefore \mathbf{H} is defined by

$$\mathbf{H} = \frac{\mathbf{L} + \mathbf{V}}{2} \quad (3.7)$$

The specular term in Phong's model then becomes

$$I_{\text{specular}} = I_i k_s (\mathbf{N} \cdot \mathbf{H})^n \quad (3.8)$$

Cook and Torrance [Cook82] extended this model to account for the spectral composition of highlights – their dependency on material type and the angle of incidence of the light. These advances have a subtle effect on the size and colour of a highlight compared to that obtained from the Phong's model. This model is most successful in rendering shiny metallic-like surfaces

In the next section, we will discuss the Lambertian illumination model which is used in this thesis. The Lambertian illumination model is the simplest type of reflection. It does reasonably well in approximating reflection for a matte surface that looks the same from all directions. It is widely used in the field of computer vision as a simple model.

3.2.2. Lambertian Illumination Model

First of all, consider diffuse – optically rough – surfaces reflecting a portion of the incoming light with radiant intensity uniformly distributed in all directions. A Lambertian surface will look equally bright from any direction for any illumination

direction. In other words, the reflected intensity is independent of the viewing direction. Examples of such surfaces include cotton cloth, many carpets, matte paper and matte paints.

However, the intensity does depend on the light source's orientation relative to the surface. Mathematically, this is represented as the dot product of the surface derivative vector with the illuminant vector, and this forms Lambert's Law.

$$i(x, y) = \rho\lambda(\mathbf{N} \cdot \mathbf{L}) = \rho\lambda \frac{-p \cos \tau \sin \sigma - q \sin \tau \sin \sigma + \cos \sigma}{\sqrt{p^2 + q^2 + 1}} \quad (3.9)$$

where

- $i(x, y)$ is the image intensity;
- $\mathbf{N} = \left(\frac{-p}{\sqrt{p^2 + q^2 + 1}}, \frac{-q}{\sqrt{p^2 + q^2 + 1}}, \frac{1}{\sqrt{p^2 + q^2 + 1}} \right)$ is the unit vector normal to the surface $s(x, y)$ at the point (x, y) ;
- $p = \frac{\partial s(x, y)}{\partial x}$ and $q = \frac{\partial s(x, y)}{\partial y}$ are surface partial derivatives measured along the x and y axes, respectively;
- $\mathbf{L} = (\cos \tau \cdot \sin \sigma, \sin \sigma \cdot \sin \tau, \cos \sigma)$ is the unit vector towards the light source;
- σ and τ are the illuminant vector's slant and tilt angles defined in *Figure 3. 2*;
- ρ is surface albedo, a material dependent coefficient;
- and λ is the strength of the light source.

To use Lambertian law we have to make the following assumptions:

- 1) The surface is *ideally diffuse*, where the incident light is equally re-distributed in all directions, and its reflectance function is uniform. The situation where the surface is non-uniform can be dealt with using ρ and λ .
- 2) The viewer is far away from the surface relative to the size of test surface, so that orthographic projection in the image system can be assumed.
- 3) Light sources are supposed to be infinity from the surface, such that the light source energy does not depend on the position of the surface. In other words, it assumes that illumination is constant over the whole surface.

- 4) For a perfect Lambertian model, both *self* and *cast shadows* are ignored, as well as *inter-reflections*.
- 5) We only consider the angle of incidence θ from 0 to 90 degrees. Greater angles (where the $N \cdot L$ is negative) are blocked by the surface and the reflected energy is 0 . The light is incident on the back of the surface, meaning it is blocked by the object.
- 6) It is obvious that the Lambertian model cannot describe *specular* reflections, or *highlights*, which occur at places where the direction of direct reflection equals the viewing direction.

The Lambertian model has been shown to describe diffuse reflection reasonably well. It was used by Woodham [Woodham80] to determine surface shape by using the photometric stereo. Coleman and Jain [Coleman82] extend photometric stereo to four light sources, where specular reflections are discarded and estimation of surface shape can be performed by means of diffuse reflections and the Lambertian model. Nayar, Ikeuchi and Kanade [Nayar90] developed the photometric approach which uses a linear combination of Lambertian and an impulse specular component to obtain the shape and reflectance information for a surface.

3.3. Kube-Pentland Surface Model

Kube and Pentland [Kube88] present a spectral model for the formation of the image from an illuminated fractal surface. It is shown that the power spectral density is a function of the illumination angles and therefore extrinsic in nature, while the fractal dimension on the other hand is purely a function of the original surface and is therefore an intrinsic texture measure. Therefore, Kube and Pentland's surface model will be used in this thesis.

3.3.1. Theory

- **Assumptions**

This theory assumes the following:

- 1) The surface reflectance is Lambertian;
- 2) An orthographic camera model;
- 3) A viewer-centred co-ordinate system, in which the reference plane of the surface is perpendicular to the viewing direction;
- 4) Surface albedo is constant.
- 5) A constant illumination vector over the surface;
- 6) The illumination vector is not close to the viewing direction;
- 7) Shadows and specularities are two aspects of real illumination not predicted by the model;
- 8) Inter-reflection is not predicted too.
- 9) The surface slope angles are small and the surface is smoothed sufficiently for it to be differentiable.

- **Kube's linear reflectance model**

Kube and Pentland's model predicts that the intensity will approximate a linear combination of the surface derivatives. Now we recall the Lambertian reflectance model in equation (3. 9), where the image $i(x,y)$ can then be expressed as a function of the illuminant orientation (τ, σ) and the surface derivative fields, $p(x,y)$ and $q(x,y)$ where $\rho\lambda=1$. This results in a non-linear operation at each facet. Taking the MacLaurin expansion of $\frac{1}{\sqrt{p^2 + q^2 + 1}}$ in the equation (3. 9) and yields

$$i(x,y) = (-p \cos \tau \sin \sigma - q \sin \tau \sin \sigma + \cos \sigma) \left[1 - \frac{p^2 + q^2}{2!} + \frac{9(p^2 + q^2)^2}{4!} \dots \right] \quad (3. 10)$$

Using the first three terms forms a linear estimate

$$i(x,y) = -p \cos \tau \sin \sigma - q \sin \tau \sin \sigma + \cos \sigma \quad (3. 11)$$

or

$$I = \begin{bmatrix} p \\ q \\ 1 \end{bmatrix} \begin{bmatrix} -\cos \tau \sin \sigma & -\sin \tau \sin \sigma & \cos \sigma \end{bmatrix} \quad (3. 12)$$

where the approximation is reasonable at $p \gg p^2$ and $q \gg q^2$ (i.e. p and q are small) so that the quadratic and higher order terms can be neglected. The form of Kube's model is optimal in the least squares sense [McGunnigle98]. Chantler reported that the error introduced by this approximation for a slant angle of 15° is 3.5% in [Chantler94a]. It is also noted that if the slant angle σ becomes small, $\sin \sigma \approx \theta$ and this means that the quadratic terms in equation (3. 10) cannot be neglected. Kube therefore further assumes $\sin \sigma > 0.1$, i.e. the illuminant vector \mathbf{L} is not within 6° of the z axis [Kube88].

3.3.2. Frequency Domain Responses

More specifically, an expression for the spectrum of the image is developed in terms of the surface texture's spectrum and illuminant vectors. We note that since differentiation is a linear operation, equation (3. 11) can be transformed into the frequency domain and expressed as a function of the surface magnitude spectrum while discarding the constant term [Chantler94a] [McGunnigle98]:

$$I_m(\omega, \theta) = i \cdot \omega \cdot \sin \sigma \cdot \cos(\theta - \tau) \cdot S_m(\omega, \theta) \quad (3. 13)$$

where

- $I_m(\omega, \theta)$ is the image magnitude spectrum;
- $S_m(\omega, \theta)$ is the surface magnitude spectrum;
- ω is the angular frequency of the Fourier component;
- θ is its direction with respect to the x -axis;
- i represents a 90° phase shift; and
- σ and τ are the illuminant vector's slant and tilt angles

This equation can be divided into three components:

1. the surface response $I_{ms}(\omega, \theta) = [i \cdot \omega \cdot S_m(\omega, \theta)]$;

2. the tilt response $I_{m\tau}(\omega, \theta) = [\cos(\theta - \tau)]$; and
3. the slant response $I_{m\sigma}(\omega, \theta) = [\sin\sigma]$.

For the purposes of this thesis it is more helpful to express equation (3. 13) in terms of the power spectrum:

$$I(\omega, \theta) = \omega^2 |\sin \sigma|^2 |\cos(\theta - \tau)|^2 S_{\varphi}(\omega, \theta) \quad (3. 14)$$

where

- (ω, θ) is the polar form of spatial frequency with $\theta=0^\circ$ being the direction of the x -axis;
- $I(\omega, \theta)$ is the image power spectrum, and
- $S_{\varphi}(\omega, \theta)$ is the surface power spectrum of a surface orientated at φ . Note that surface orientation φ and direction of spectrum θ are on the same plane x - y with respect to the x -axis.

This equation contains simple trigonometric terms, which enable the directional effect of illumination to be more easily understood. Since we are interested in surface rotation, we only deal with the effects of the $|\cos(\theta - \tau)|^2$ term, which is a directional filter and is independent of radial frequency ω .

3.3.3. Directional Filter

- ***Surface rotation vs. image rotation.***

If we consider only the directional aspects of equation (3. 14) we can see that the image directionality is a product of the illuminant tilt angle τ and the surface directionality. In this way a surface rotation may not be equivalent to image rotation if the illuminant is not also rotated. The directionality in the image of a directional surface is the product of both the surface and illuminant directionalities.

If the surface is an isotropic one, then the surface rotation will have no significant effect on the image directionality as long as the illuminant direction is held constant.

On the other hand, if the surface is a directional one, the surface rotation will alter the imaged texture beyond simple rotation. This means that a rotated directional surface is distinctly different in appearance compared to the unrotated surface. Both of these effects can be seen in *Figure 3. 9*.

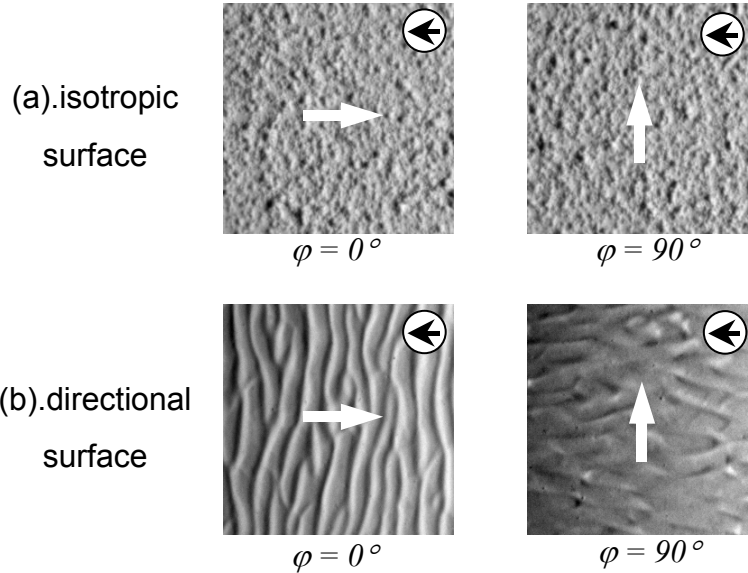


Figure 3. 8 Isotropic surface and directional surface with rotation $\varphi=0^\circ$ and 90° (indicated by the white arrows in the centre). The illuminant tilt is kept constant at $\tau=0^\circ$ (indicated by the black arrows in white circles).

- ***Illumination directional filter.***

In equation (3. 13), the most important feature of Kube's model is the term $I_{mr}(\omega,\theta)=[\cos(\theta-\tau)]$, which predicts the effect of illumination directional filter in Kube's model. This can be understood by considering *Figure 3. 8*. We may see that, for an isotropic surface, image directionality is only due to the directional effect of the illuminant. Therefore, changing the illuminant directions causes a change in the direction of energy in the corresponding power spectral density (PSD). Furthermore, the highest texture energy lies in the direction of the illuminant tilt angle τ .

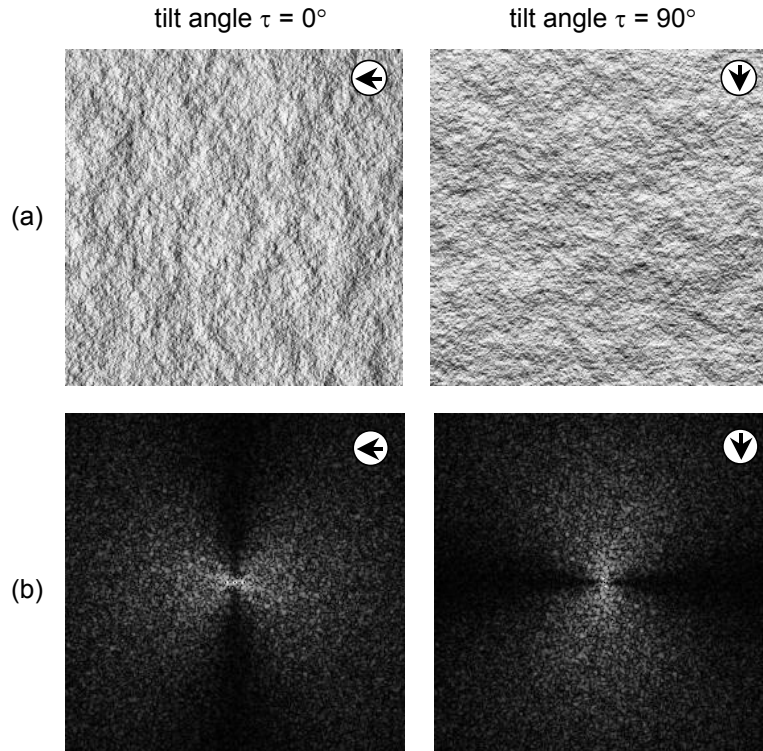


Figure 3. 9 A fractal surface of “rock” rendered by Kube’s model (a). Surfaces at two different illumination directions (tilt angle of $\tau=0^\circ$ and $\tau=90^\circ$, indicated by the black arrows in white circles); (b). the corresponding power spectral density.

- ***Image variance is not a surface rotation invariant feature for directional surfaces***

There is a problem in the case of directional surfaces, where the image variance will vary with the rotation of the directional surface. Depending on the degree of directionality, the variation in image variance may cause the classifier to fail. In this case, the image variance is not a surface rotation invariant feature for directional surfaces [Chantler94b] [McGunnigle99a].

With regard to the equation (3. 14), the image variance is the integral of the image power spectrum, assuming the mean component to be equal to zero. The following can therefore be obtained:

$$\sigma^2(\varphi) = \int_0^\infty \omega^3 \sin^2(\sigma) \cdot 2 \int_0^\pi \cos^2(\theta - \tau) \cdot S_\varphi(\omega, \theta) d\theta d\omega \quad (3. 15)$$

If we consider a new axis with the direction of the unidirectional surface texture where $\theta^* = \theta - \varphi$, and then equation (3. 15) becomes:

$$\sigma^2(\varphi) = \int_0^\infty \omega^3 \sin^2(\sigma) \cdot 2 \int_{-\varphi}^{\pi-\varphi} \cos^2(\theta^* + \varphi - \tau) \cdot S_\varphi(\omega, \theta^*) d\theta^* d\omega \quad (3. 16)$$

Now if the inner integral part of the equation (3. 16) is taken into account:

$$\begin{aligned} & 2 \int_{-\varphi}^{\pi-\varphi} \cos^2(\theta^* + \varphi - \tau) \cdot S_\varphi(\omega, \theta^*) d\theta^* \\ &= \int_0^\pi [1 + \cos(2\theta^* + 2\varphi - 2\tau)] \cdot S_\varphi(\omega, \theta^*) d\theta^* \\ &= \int_0^\pi S_\varphi(\omega, \theta^*) d\theta^* + \int_0^\pi \cos(2\theta^* + 2\varphi - 2\tau) \cdot S_\varphi(\omega, \theta^*) d\theta^* \\ &= \int_0^\pi S_\varphi(\omega, \theta) d\theta \\ &+ \int_0^\pi [\cos 2\theta \cdot \cos(2\tau - 2\varphi) + \sin 2\theta \cdot \sin(2\tau - 2\varphi)] \cdot S_\varphi(\omega, \theta) d\theta \end{aligned} \quad (3. 17)$$

Therefore equation (3. 15) can be simply expressed in the form of

$$\begin{aligned} \sigma^2(\varphi) &= A + [B \cos(2\tau - 2\varphi)] + [C \sin(2\tau - 2\varphi)] \\ &= A + [D \cos(2\tau + \phi)] \end{aligned} \quad (3. 18)$$

where

$$\begin{aligned} A &= \sin^2(\sigma) \int_0^\infty \omega^3 \int_0^\pi S_\varphi(\omega, \theta) d\theta d\omega \\ B &= \sin^2(\sigma) \int_0^\infty \omega^3 \int_0^\pi \cos 2\theta \cdot S_\varphi(\omega, \theta) d\theta d\omega \\ C &= \sin^2(\sigma) \int_0^\infty \omega^3 \int_0^\pi \sin 2\theta \cdot S_\varphi(\omega, \theta) d\theta d\omega \\ D &= \sqrt{B^2 + C^2} \\ \phi &= [\arctan(C / B)] + 2\varphi \end{aligned}$$

From equation (3. 18), we may note that

- for an *isotropic surface*, the term D will be equal to zero, and then the image variance $\sigma^2(\varphi)$ will be kept constant;
- on the other hand, for a *directional surface*, the term B will not be equal to zero and therefore image variance $\sigma^2(\varphi)$ will be a raised cosine function of surface orientation.

Figure 3. 10 illustrates the variation of image intensity variance with surface rotation for an isotropic surface “gr2” and a directional surface “wv2” (shown in Figure 3. 8 with the constant illumination tilt angle $\tau=0^\circ$). We may note that the variance of image intensity for the directional surface “wv2” is certainly not invariant to surface rotation and indeed it is following the cosine term predicted in the model. It is this directional filter effect that makes the outputs of texture features vary with the orientation of a directional surface.

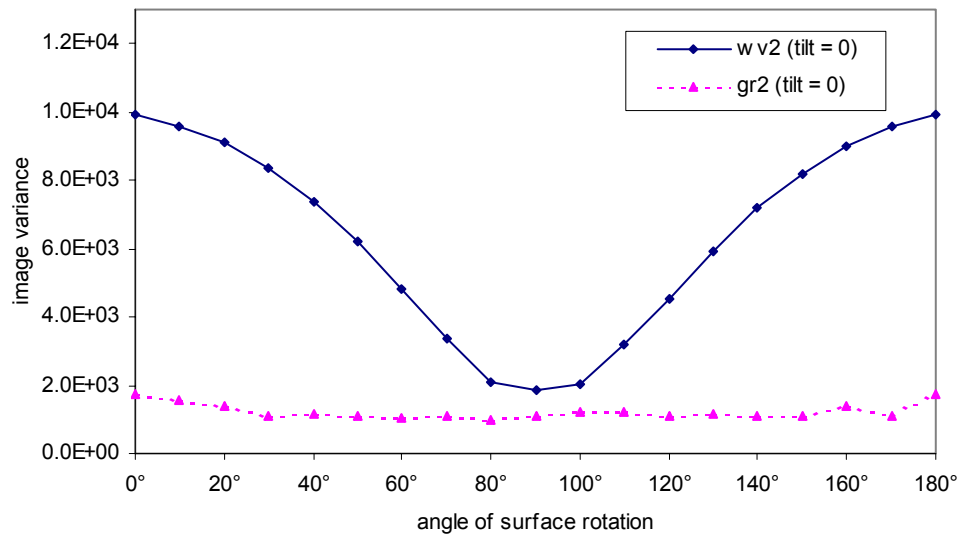


Figure 3. 10 The variation of image intensity variance with surface rotation for an isotropic surface “gr2” and a directional surface “wv2” (illumination tilt angle $\tau=0^\circ$).

3.3.4. Non-linear Effects

In this section, we investigate the non-linear effects occurring in Kube’s image model through the use of simulation. One of the reasons for this effect, is that the

quadratic and higher order terms in equation (3. 10) are neglected in developing the linear image model in equation (3. 11). Furthermore, the linear image model is based on the assumption that surface height variance is low (i.e. surface slope is less than 15 degrees) and that the slant angle does not approach 0 degrees. These assumptions are necessary to allow the Lambertian model to be linearised [Chantler94].

- ***Surface amplitude variance***

The linear image model assumes a linear relationship between the image variance and surface variance (equation (3. 13)). *Figure 3. 11* and *Figure 3. 12* show the effect of increasing the amplitude of a simple sinusoidal surface on images modelled with perfect Lambertian reflection (equation (3. 9)) and linear Lambertian reflection given by Kube's model in equation (3. 11). In order to investigate the effect of the non-linear components, we set the illumination slant angle $\sigma=45^\circ$. This angle was chosen because the reflection model assumes a \cos^2 relationship between slant angle σ and the reflected intensity, and the model seems to be most linear for a slant angle of around 45° .

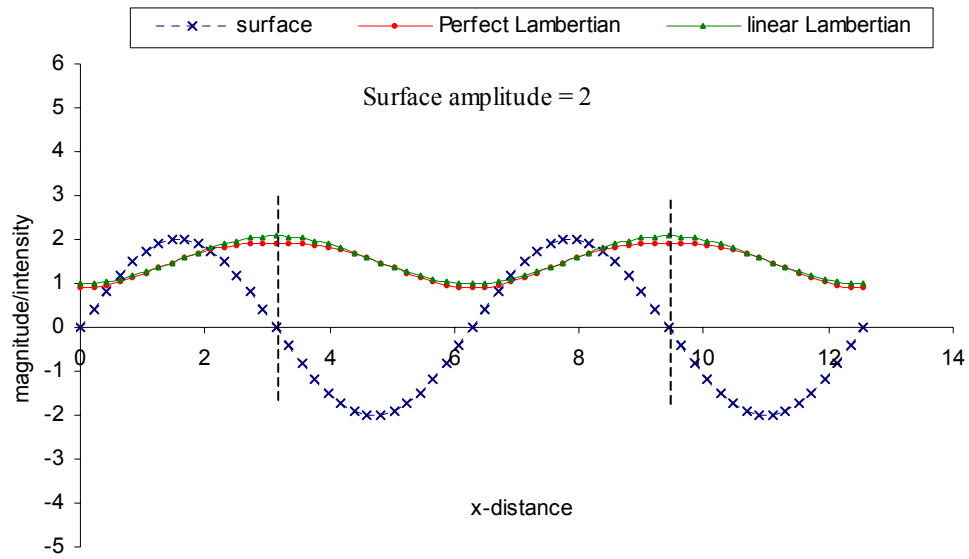


Figure 3. 11 The non-linear effects of a sinusoidal corrugated surface intensity with amplitude=2, predicted by perfect Lambertian model and linear Lambertian model ($\sigma=45^\circ$).

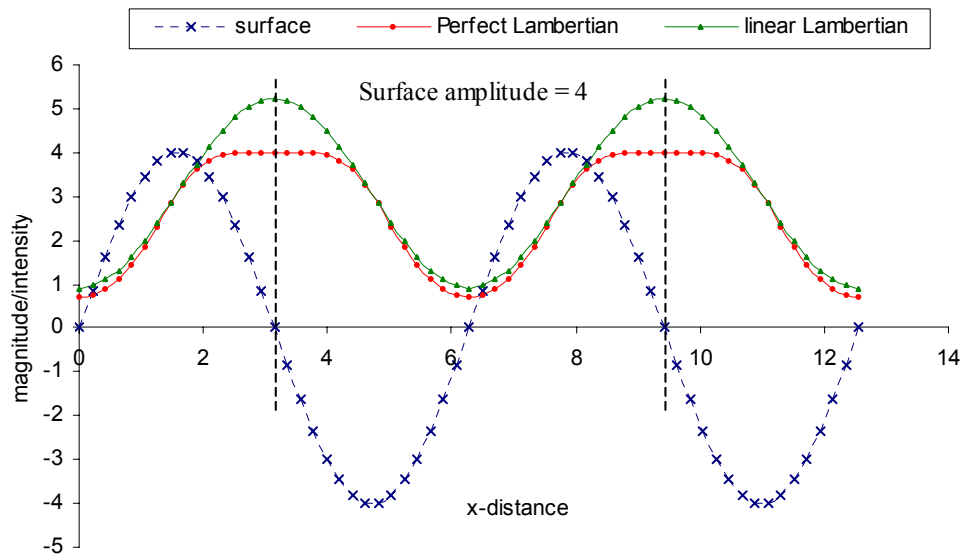


Figure 3. 12 The non-linear effects of a sinusoidal corrugated surface intensity with amplitude=4, predicted by perfect Lambertian model and linear Lambertian model ($\sigma=45^\circ$).

In both Figure 3. 11 and Figure 3. 12, it can be seen that the difference or distortion between perfect Lambertian surface and a linear Lambertian surface occurs at the position where the non-linear effects are significant, i.e. where the surface slope

angles approach their maximum values. In addition, increasing the surface amplitude from 2 to 4 accentuates these differences.

Next, we consider the situation where the illumination slant angle σ approaches the extremes i.e. 0° and 90° , such that the non-linear effect can be investigated further.

- **Frequency doubling**

For an illumination slant angle close to 0° , where the source of illumination is vertically above the surface, the equation (3. 10) becomes:

$$i(x,y)=\cos\sigma\left[1-\frac{p^2+q^2}{2!}+\frac{9(p^2+q^2)^2}{4!}\dots\right] \quad (3. 19)$$

This shows that the effect of the linear term is reduced and the higher order and quadratic terms now have a greater influence on the image intensity. An example of the frequency doubling effect of a sinusoidal corrugated surface $f(x,y)=\sin\omega x$ is shown in *Figure 3. 13*. It is illuminated at slant angle $\sigma=0^\circ$, therefore the intensity becomes dominated by the “ q ” term while the “ p ” term equals zero. This removes some of the important linear terms and leaves the intensity dependent on the non-linear term in equation (3. 20)

$$2\cos^2\omega = 1 + \cos 2\omega \quad (3. 20)$$

This shows the frequency doubling effect caused by increased distortion from the saturation of the reflection law in the testing at a sinusoidal surface in *Figure 3. 13*.

- **Clipping**

On the other hand, if the slant angle σ is increased, the reflected intensity of the surface becomes further saturated by distortion as it approaches 90° . This effect can be seen in *Figure 3. 14* where the surface is illuminated with the slant angles σ of from 40° to 80° , respectively. We may see that the *clipping* effects apparently become more severe with increasing the slant angle σ , demonstrating the non-linearity in that region.

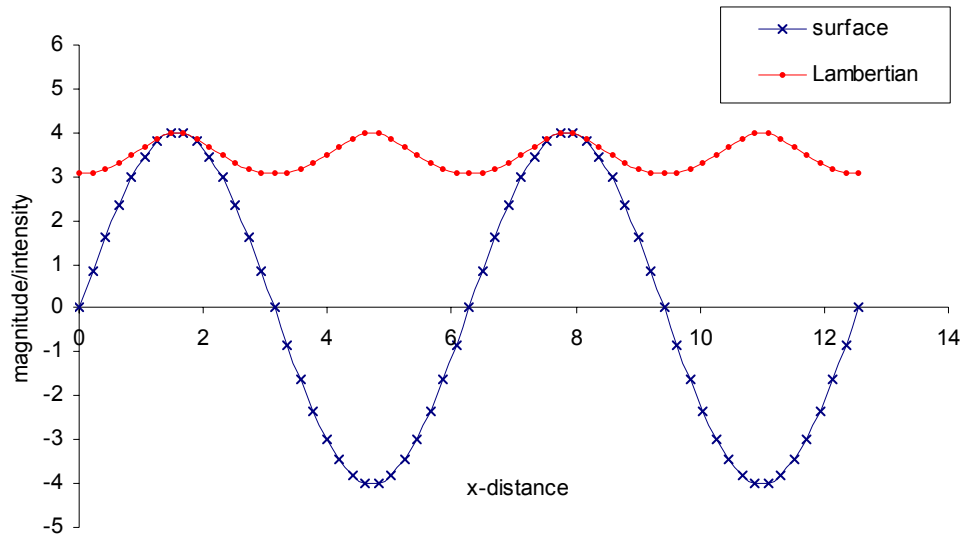


Figure 3.13 Frequency doubling effect of a sinusoidal corrugated surface illuminated at slant angle $\sigma=0^\circ$.

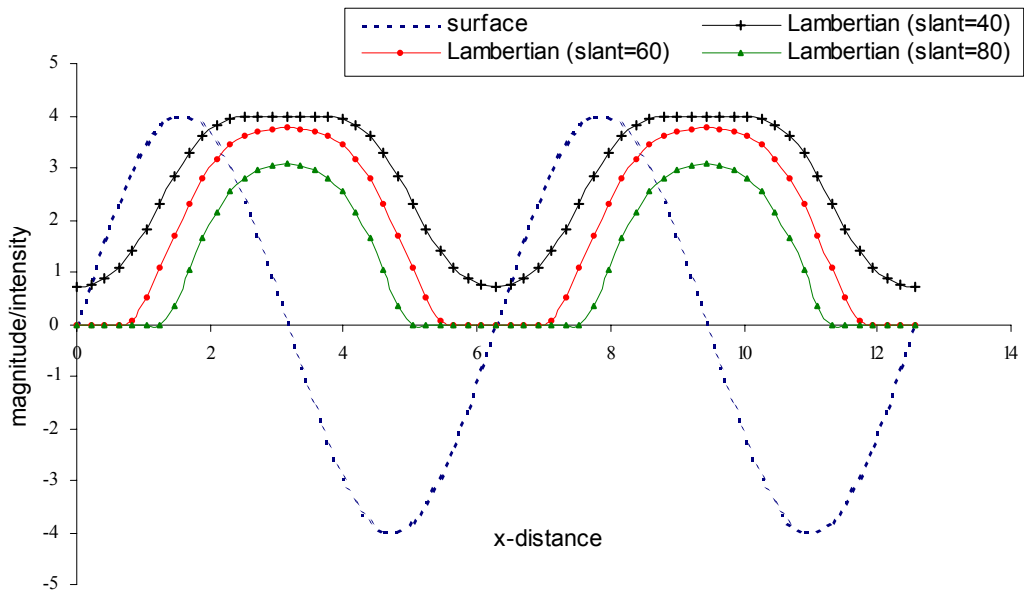


Figure 3.14 Clipping effect of a sinusoidal corrugated surface illuminated at slant angle $\sigma=40^\circ, 60^\circ$ and 80° .

3.3.5. Effect of Shadowing

Another non-linear contribution to the model is shadowing. One assumption used in our mathematical equation is Lambertian reflection where shadowing is ignored. Unfortunately in the real world shadows occur. They account for strong disagreement with the Lambertian model when real textures are used. This model is, however, a reasonable approximation of real smooth diffuse reflection given certain constraints. For a rough surface, it is acknowledged that there are significant departures from Lambert's law. Moreover, the departures are most marked for specific viewer and light source directions. The Lambertian model breaks down substantially when the angle between the view vector and the surface normal exceeds 60 degrees [Wollf98]. In this section, we will discuss the effect of shadowing on our model.

- ***Self shadow and cast shadow***

Shadows occur either at places where the path from the light source is blocked or at surfaces which are oriented away from the light source. These effect known as *cast shadow* and *self shadow*, respectively, and illustrated in *Figure 3. 15*. The two kinds of shadows also have quite different properties.

1. The *self shadow* depends on the relation between the surface normal and the lighting direction, and it is observed where the surface does not face the lighting direction.
2. On the other hand, the *cast shadow* depends on the whole 3D shape of the surface, and it is observed where the light is occluded by other objects.

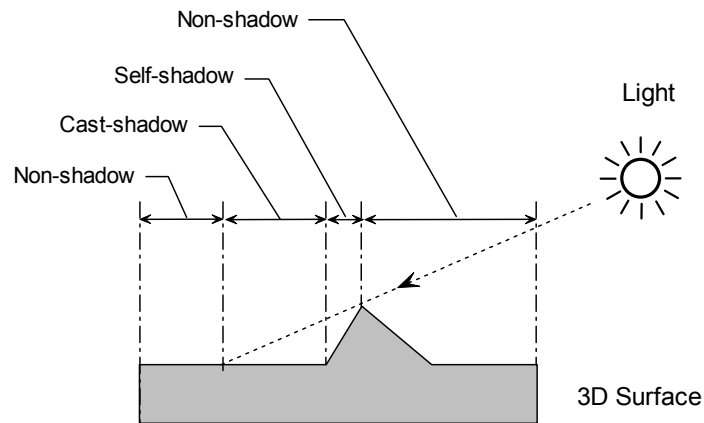


Figure 3. 15 Illustrations of cast shadow and self shadow on a 3D surface.

- ***Kube’s model rendered by the effect of shadow***

In Figure 3. 16, we simulate sinusoidal surfaces rendered by Kube’s model with the effect of shadow. An approximation to shadowing can be simply modelled in the following way: where the shadow occurs the reflected intensity is clipped and set to 0. We may clearly see that the distortions caused by the shadowing (either self or cast shadow) become more distinctive compared to that without the shadowing effect.

- ***Directional filtering effect reduces with a decrease in the slant angle σ in the case of shadow.***

As discussed in section 3.3.3 where we considered the directional filtering effect on Kube’s model and equation (3. 19), we may note that for a slant angle σ decreasing to near 0° , the effect of the linear term is reduced compared with that of the square or higher terms. Furthermore the directional filtering effect will be attenuated. Figure 3. 17 shows the effect of decreasing the slant angle σ from 70° to 10° . It is apparent that the directional filtering effect reduces as the slant angle σ approaches 0° . In addition, if the surface is rendered with the effect of shadow in Figure 3. 18, the directional filtering effect with the highest slant angle (i.e. $\sigma = 70^\circ$) is also be attenuated. In this case, the heavy shadow effects the linear approximation of Kube’s model, and the majority of the reflected intensity is clipped to 0.

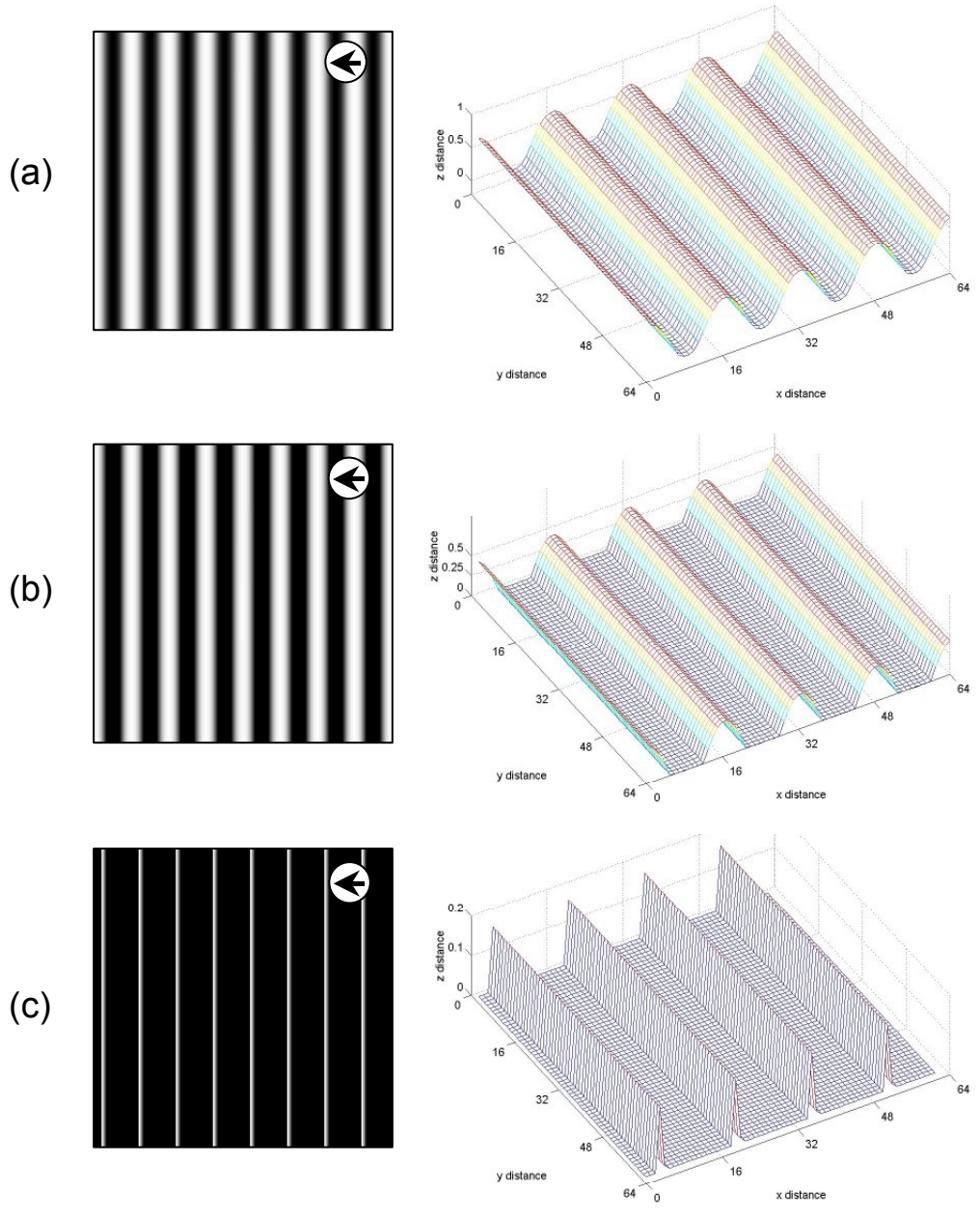


Figure 3. 16 Sinusoidal surfaces rendered by Kube's model (tilt angle $\tau=0^\circ$ and slant angle $\sigma=70^\circ$) with the effect of shadow. (a). without any shadow; (b). with self shadow only; (c). with both self and cast shadow.

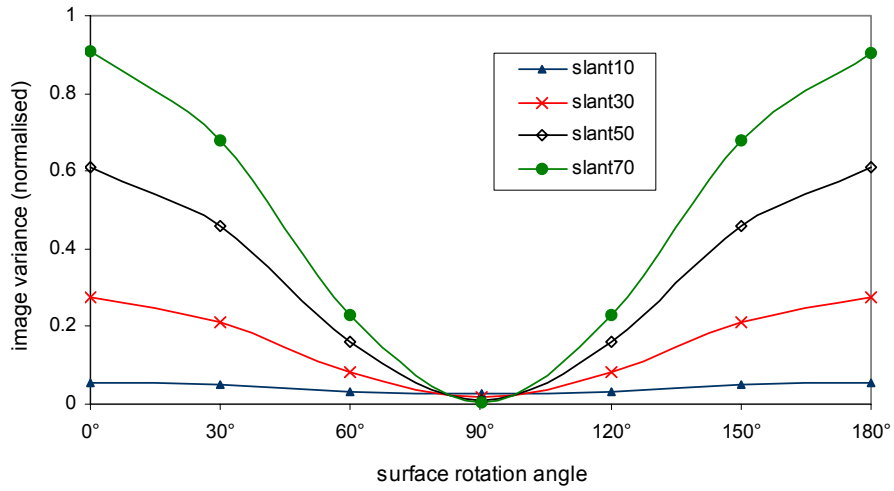


Figure 3.17 The variation of image intensity variance with surface rotation rendered over a range of illuminant slant angles and without any shadow effect (the surface is sinusoidal one rendered by tilt angle $\tau=0^\circ$).

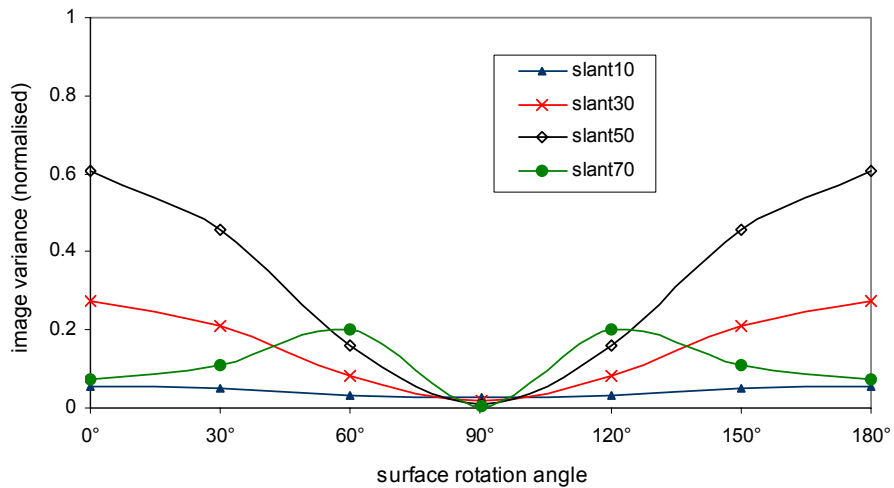


Figure 3.18 The variation of image intensity variance with surface rotation rendered over a range of illuminant slant angles and with shadow effect (the surface is sinusoidal one rendered by tilt angle $\tau=0^\circ$).

3.3.6. Summary of Kube-Pentland Model

In this section, we presented Kube and Pentland's model which predicts that the intensity approximates a linear combination of the surface derivatives. Furthermore a frequency-domain model of the image of an illuminated three-dimensional texture is

developed in terms of the surface texture's spectrum and illuminant vectors. Both its assumptions and theory are summarised. The linear approximation is reasonable at low surface slope angle.

Firstly, from this theory, the image directionality is a product of the illuminant direction and surface directionality. As a result, a surface rotation is not equivalent to an image rotation if the illuminant is not rotated. It also can be seen that the directional filter characteristics of an image for an isotropic surface are described by the term of $\cos(\theta - \tau)$. This predicts that the directionality of an image can be described by a cosine function. In addition, for an isotropic surface, the image variance will be kept constant; while for a directional surface, the image variance is a raised power cosine function of surface rotation. Hence we note that image variance is not a surface rotation invariant feature for a directional surface, which leads to surface-based classification rather than image-based classification.

Secondly, the non-linear effects neglected by the Kube's model are considered. Their effect on surface amplitude variance, frequency doubling and intensity clipping is investigated through the use of simulation. This confirms Kube's linear model must be used on the basis that surface height variance is low and that the slant angle does not approach 0 degrees.

Lastly, the shadowing contribution to the model is shown, as shadowing can not be ignored in the real world.

3.4. Descriptions of Synthetic Surface

In this section, we briefly introduce four models of rough synthetic surfaces, which are used in the whole of this thesis for the purpose of simulation.

If we consider a texture to be a realisation of a two dimensional random process the texture can be described by its mean and its phase. For a *structured surface*, there is

important information in its phase spectrum. However for *unstructured surfaces* the phase spectrum is assumed to be equally distributed. In this thesis, we only deal with unstructured synthetic surfaces so that the phase spectrum is neglected.

In texture analysis, the fractal model is one of the most commonly used: the texture is viewed as the realisation of a random process. To characterise the texture, the fractal dimension has to be estimated. A fractal function is good for modelling 3D real surfaces because many physical processes produce a fractal surface shape. Indeed fractals are widely used as a graphics tool for generating natural-looking shapes. A survey of natural imagery has shown that the 3D fractal surface model furnishes an accurate description of both texture and shaded image regions [Pentland88].

Four surface models have been proposed that are defined in terms of the power spectrum. They are the 2D forms of the fractal [Pentland88], Mulvanney [Mulvanney89], Ogilvey [Sayles78] and sand ripple [Linnett91], where the fractal and Mulvanney surface are isotropic, while the Ogilvey and sand ripple are directional ones. They are defined as follow:

- **Fractal**
$$S_{Fractal}(\omega) = \frac{k_{rock}}{\omega^3} \quad (3.21)$$

where $S(\omega)$ is two dimensional power spectrum; ω is the radial frequency and k_{rock} is a constant.

- **Mulvanney**
$$S_{Mulvanney}(\omega) = k_{malv} \left(\frac{\omega^2}{\omega_c^2} + 1 \right)^{-3/2} \quad (3.22)$$

where ω_c is the cut-off frequency and k_{malv} is a constant.

- **Ogilvey**
$$S_{Ogilvey}(u, v) = \frac{k_{ogil}}{(u_c^2 + u^2)(v_c^2 + v^2)} \quad (3.23)$$

where u and v are Cartesian frequency coordinates; u_c and v_c are cut-off frequencies in the x and y directions and k_{ogil} is a constant.

- **Sand ripple**
$$S_{sand}(u, v) = \frac{k_{sand}}{\left[\sqrt{(u - \omega_c)^2 + (v - \omega_d)^2} \right]^3} \quad (3.24)$$

where u and v are Cartesian frequency coordinates; ω_c and ω_d are cut-off frequencies in the x and y directions and k_{sand} is a constant.

Images of these surfaces rendered with the Lambertian model are shown in *Figure 3.19*. Note that in the rest of this thesis, we denote fractal surface as “*rock*”, Mulvanney surface as “*malv*”, Ogilvey surface as “*ogil*” and sand ripple as “*sand*”.

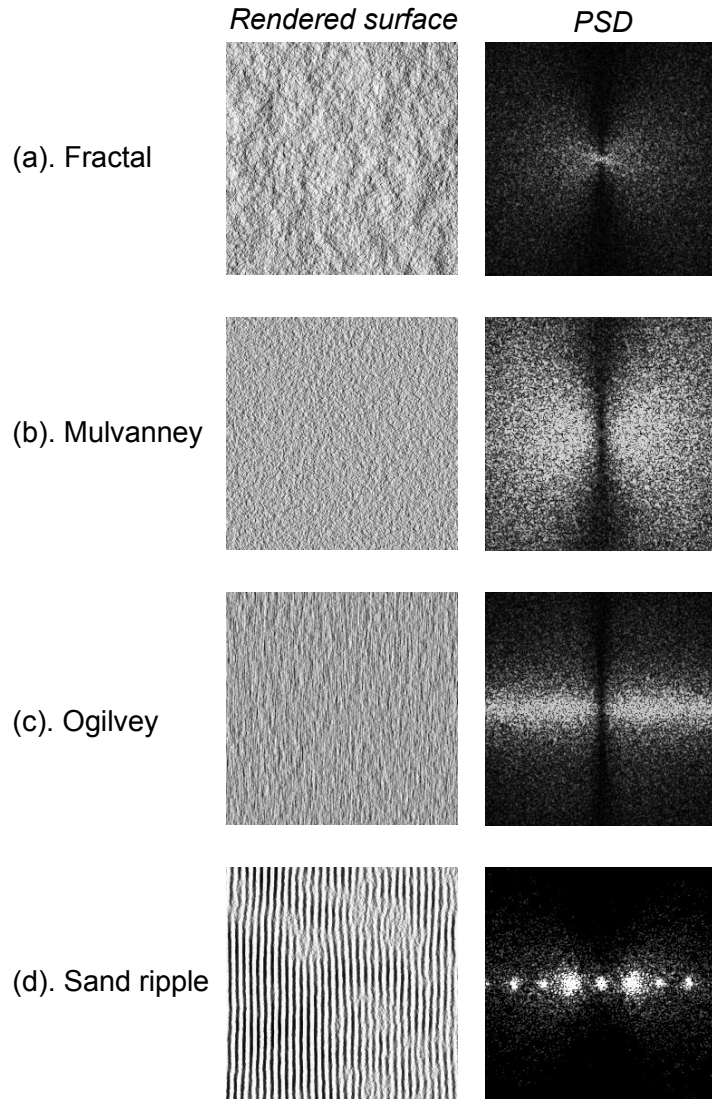


Figure 3.19 Four synthetic textures rendered with a Lambertian model and their corresponding surface height PSD.

3.5. Image-based Classification vs. Surface-based Classification

Many texture classification schemes have been presented that are invariant to image rotation [Port97a] [Cohen91] [Mao92]. They normally derive their features directly from a single image and are tested using rotated images. If the image texture results solely from albedo variation rather than surface relief or if the illumination is not directional or immediately overhead, then these schemes are surface-rotation invariant as well. However, in many cases *rotation of a textured surface produces images that differ radically* from those provided by pure image rotation (an example can be seen in *Figure 3. 8*). This is mainly due to the directional filtering effect of imaging using side-lighting, described by Kube's frequency model in equation (3. 13). Therefore, a distinction between classifying a surface using measured pixel intensities and classifying on the basis of the reflectance function is apparent.

Kube and Pentland [Kube84] identified and verified a frequency domain model of the image formation process for 3D surface texture. This has shown that the imaging process acts as a directional filter of texture and that changes in illuminant direction can cause catastrophic failure of classifiers [Chantler94b] [McGunnigle98]. Chantler [Chantler94] has used Kube's model to remove the directional effect associated with illumination in his scheme which estimates a quantity that is independent of the orientation of the surface and relative to the illuminant. However, there are two main weaknesses that stem from the linearization of Kube's model. The scheme is firstly unable to deal with the situation where the surface normal is perpendicular to illuminant direction. Secondly, only some classes of surfaces are suitable to the use of a linear model. Based on these reasons, this theme is not sufficiently robust with regard to the rotation of texture. However a new methodology [McGunnigle00] was developed for texture classification based on the direct use of surface gradient and surface reflectance information which used photometric stereo to extract and separate surface relief and albedo information. This enables classification to be performed by comparing texture features computed directly from surface properties rather than image intensity values.

An example of classification accuracy for image rotation and surface rotation is given in *Figure 3. 20*. The statistical classifier is used on a set of isotropic Gabor filters where the features contain no information about the directionality of the texture so that they are rotation insensitive features. The detailed structure of the rotation insensitive classifier can be found in [McGunnigle99a]. The four synthetic test textures used in this experiment are described in the previous section of this chapter. First of all, the image is rotated and then the conventional rotation invariant algorithms are tested. Secondly, the surface is rotated and rendered by Kube's model under the same illuminant condition. From the classification accuracy in *Figure 3. 20*, we may see that the conventional rotation invariant algorithms are not able to deal with the surface rotation compared to those utilising image rotation. In our experiments with data sets at surface rotation $\varphi=0^\circ$, the prominent directionality of the surface is perpendicular to the illuminant direction. Therefore at surface rotation $\varphi=90^\circ$, surface directionality and illuminant direction are the same. This effect makes the discrimination more difficult and the classification accuracy was found to decrease significantly. This again demonstrates that surface rotation is not equivalent to image rotation for 3D surfaces.

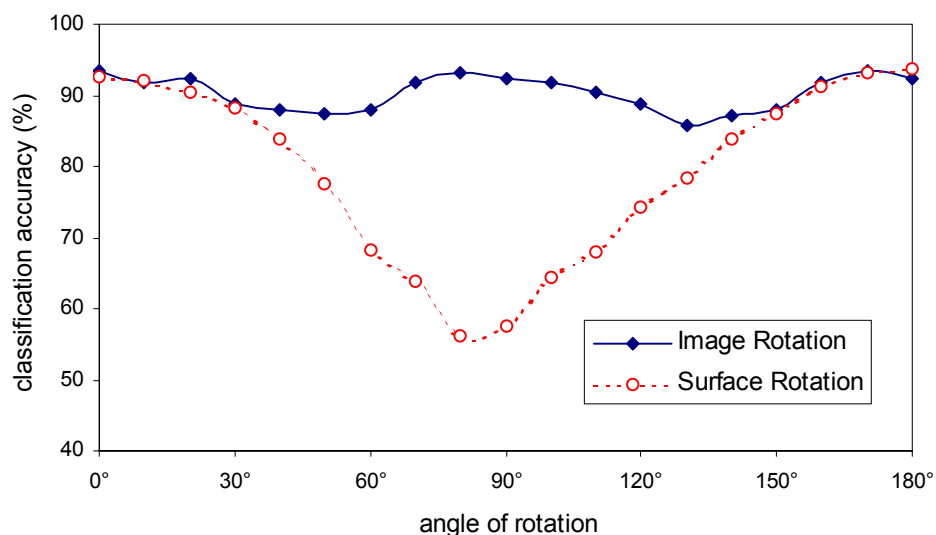


Figure 3. 20 Classification accuracy for image rotation and surface rotation.

3.6. Summary

In this chapter, the process from surface to image is reviewed. First of all, the surface roughness models were discussed, illumination geometry defined and diffuse and specular reflectance were considered. A review of related work on reflection and illumination modelling was given. Afterwards, a simple Lambertian illumination model was selected. It is proven to describe diffuse reflection reasonably well.

We presented Kube's model, a linear Lambertian model, which assumes fixed illumination and viewing geometry and expresses observed intensity as a linear function of surface partial derivatives. We model all the surfaces as Lambertian. Most of the surfaces have moderate slopes and can be accurately rendered using a linear approximation. From this model, one characteristic of rough surface textures is that the appearance of the surface is a function of the illuminant direction as well as of the surface topography. Furthermore, Kube's model functions as a directional filter. In addition, the non-linear effects neglected by the model were investigated. With regard to surface amplitude variance, they are frequency doubling and intensity clipping. Finally the shadowing contribution to the model was also shown.

We briefly introduced four models of rough synthetic surfaces, which are used in the throughout this thesis for the purpose of simulation. They are the 2D forms of the fractal, Mulvanney, Ogilvey and sand ripple.

We demonstrated that the rotation of a directional surface is not equivalent to the rotation of its image. Therefore a surface rotation invariant classifier must take this effect into account. One approach is to classify using the properties of the surface rather than those of the image. If the properties of the surface can be estimated, it may be possible to improve the performance of the classifier. We will introduce the *photometric stereo* technique in the next chapter, which will enable us to directly estimate surface properties from several images illuminated under different lighting sources.